R-35

GROWTH AND CHARACTERIZATION OF MATERIALS FOR TUNABLE LASERS IN THE NEAR INFRARED SPECTRAL REGION

PRRINCIPAL INVESTIGATORS: Richard C. Powell
and
Joel J. Martin

CONTRACTOR: Oklahoma State University
Department of Physics
Stillwater, OK 74078-0444

SEMI-ANNUAL PROGRESS REPORT: 1 February 1989 - 31 July 1989

GRANT NUMBER: NAG-1-694

FOR: NASA Langley Research Center
Langley, VA 23665

I - SUMMARY

During this report period research was performed in three areas: laser spectroscopy, crystal growth, and radiation damage. The key personnel involved in the laser spectroscopy work were Prof. R.C. Powell (P.I.) and M.L. Kliewer (G.R.A.) while the key personnel involved in the crystal growth and radiation damage work were Prof. J.J. Martin (P.I.) and D.L. Hart (G.R.A.).

The laser spectroscopy effort focused on understanding the effects of excited state absorption processes involving pump photons. This work was performed on a variety of rare earth ions in different hosts. The crystal growth and radiation damage efforts focused on $LiYF_4$ (YLF) doped with rare earth ions. The results of this work are described in the following sections.

During the next report period the work in all three areas will focus on rare earth ions in YLF.

II. LASER SPECTROSCOPY

During this report period the laser spectroscopy work involved two projects related to trying to understand the effects of excited state absorption of pump photons on laser-pumped laser operation. The first of these was developing a detailed theoretical model to explain the experimental results described in the last report. This used Nd^{3+} in various host materials as an example of these processes. The details of this model are given below. The second project was obtaining experimental results on the laser-pumped laser characteristics of Er^{3+}-doped materials. The results these measurements will be described in the next report.

A Model Describing the Effects of Excited State Absorption of Pump Radiation on Laser-Pumped Lasers

Introduction

Results of an investigation of the spectral dynamics of an $Y_3Al_5O_{12}:Nd^{3+}$ (Nd-YAG) laser pumped by an alexandrite laser have been reported recently.[1] In this paper we develop the theory to quantitatively explain the change in slope efficiency with change in pumping wavelength in Nd-YAG and conclusions are extrapolated to other neodymium doped materials. These results show important differences between broadband frequency pumping and monochromatic pumping, demonstrate the importance of completely characterizing the pumping dynamics of laser systems, and show the effects of

excited state absorption (ESA) of pump photons on the slope efficiency of the laser operation.

An alexandrite laser with a spectral width of 1 nm FWHM and an output tunable between 725 and 805 nm was used to pump a Nd-YAG crystal. The tunability of the alexandrite laser was extended past wavelengths reported earlier [1] on the low energy side with the use of a different high reflector and ouput coupler making it possible to pump directly into the $^4F_{5/2}$ level of neodymium. The pulse width of the alexandrite was 60 μs FWHM and the maximum power obtainable was 20 W at a repetition rate of 20 Hz at the peak of the gain curve of the alexandrite laser.

The crystal was mounted in a cavity of length 24 cm consisting of a 100 % reflector with a 50 cm radius of curvature and a flat 85 % output coupler. Transverse pumping was employed with cylindrical and convex lenses to focus the pump laser beam in a line the length of the Nd-YAG sample. Several spatial modes were present in the Nd-YAG laser output and the radius of the area encompassing these modes was measured to be 0.07 cm. This value was used for the cavity waist in the calculations of the absorbed power by the material and the pump beam was focused within this waist. The small

beam waist insures uniform population inversion within the mode volume and that all of the pump energy entering the crystal will pass through the mode. The power incident on the Nd-YAG crystal and the power output from the Nd-YAG laser were measured simultaneously with two calibrated power meters. The Fresnel reflections and absorption of the material were considered when calculating the power absorbed by the crystal. The sample was 0.28 cm long and contained approximately 10^{20} Nd^{3+} ions/cm^3.

Figure 1 shows the energy levels of Nd^{3+} and the relevant electronic transitions when pumping with 754 and 791 nm. The alexandrite laser output is tuned over the absorption transitions shown in Fig. 1 after which radiationless relaxation occurs to the $^4F_{3/2}$ metastable state. Fluorescence is observed from the $^4F_{3/2}$ level to the levels belonging to the ^4I_J terms and, above threshold, lasing occurs in the $^4F_{3/2} \rightarrow {}^4I_{11/2}$ transition.

The room temperature fluorescence spectra between 300 and 900 nm of Nd-YAG pumped by an alexandrite laser at 734 and 749 nm have been reported previously.[1] Along with the normal fluorescence from the $^4F_{3/2}$ level in the near infrared spectral region, strong emission lines appear at higher energies between about 380 and 600 nm. These transitions are associated

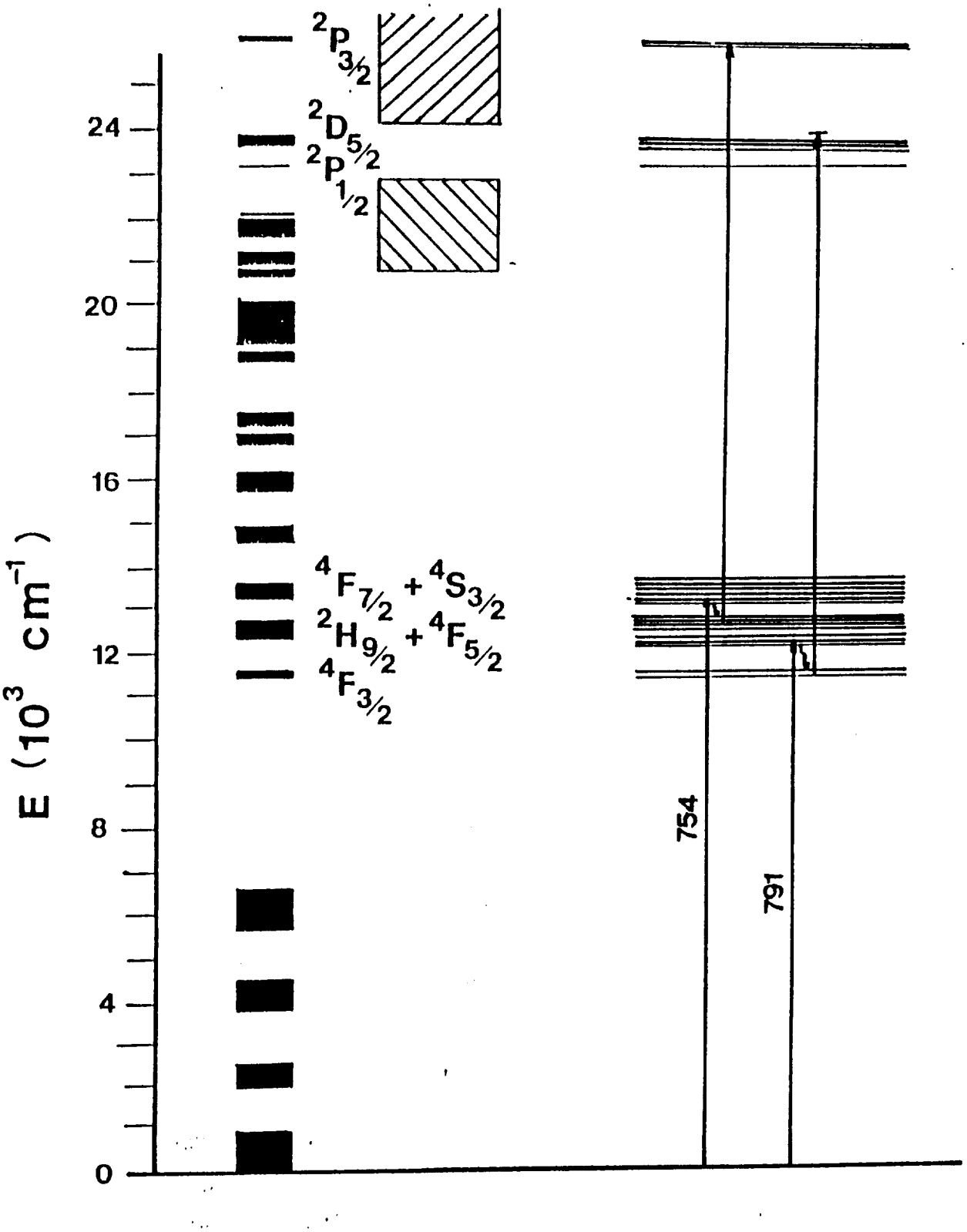

FIG. 1. Energy level diagram of Nd^{3+} in YAG.

with multi-photon absorption processes. The specific transitions that appear in this spectral region and their relative intensities depend on the wavelength and the power of the pump pulse. These transitions originate from the $^2P_{3/2}$, $^2D_{5/2}$, and $^2P_{1/2}$ levels and terminate on the various multiplets of the ground term.

The emission in the spectral region from approximately 500 to 700 nm can be explained with the absorption of a lasing photon by one of the states of lower energy than the pump photon. However, in order to excite the higher lying fluorescence levels producing the emission in the spectral region from 300 to 500 nm, it is necessary for two pump photons to be absorbed. Conservation of energy requires that the energy of the transition from the ground state to the final level must match the sum of the energies of the two photons minus any energy lost through radiationless decay processes. As reported earlier [1], there are only two paths for the required two-photon excitation process under these pumping conditions. One path has the first photon absorbed by a transition to a Stark component of the $^4F_{7/2}+^4S_{5/2}$ levels followed by radiationless relaxation to the levels of the $^2H_{9/2}+^4F_{5/2}$ manifold. The second photon is absorbed before the ion can continue relaxing

down to the $^4F_{3/2}$ metastable state. Depending on the exact energy of the pump photons, there is a good energy match to transitions terminating on the two Stark components of the $^2P_{3/2}$ level. In this level there is a branching ratio for fluorescence and radiationless relaxation to the lower $^2D_{5/2}$ and $^2P_{1/2}$ levels from which some fluorescence also occurs. A second path for two photon excitation has absorption of a pump photon occurring after relaxation to the $^4F_{3/2}$ metastable state. This is not completely unexpected considering the long lifetime of that level. For most host materials the energy difference between the $^4F_{3/2}$ metastable level and upper states of Nd^{3+} will not exactly match the energy of the pump photons however this energy mismatch can be compensated for with phonon energy of the lattice.

Theoretical Model Used to Describe Pump Photon ESA

Rate equations were used to model the pumping dynamics occurring when excited state absorption of pump photons takes place. The usual four level laser system that is used to describe Nd^{3+} lasers[2] is expanded to include two additional levels for the modeling of ESA of pump photons. Figure 2 shows

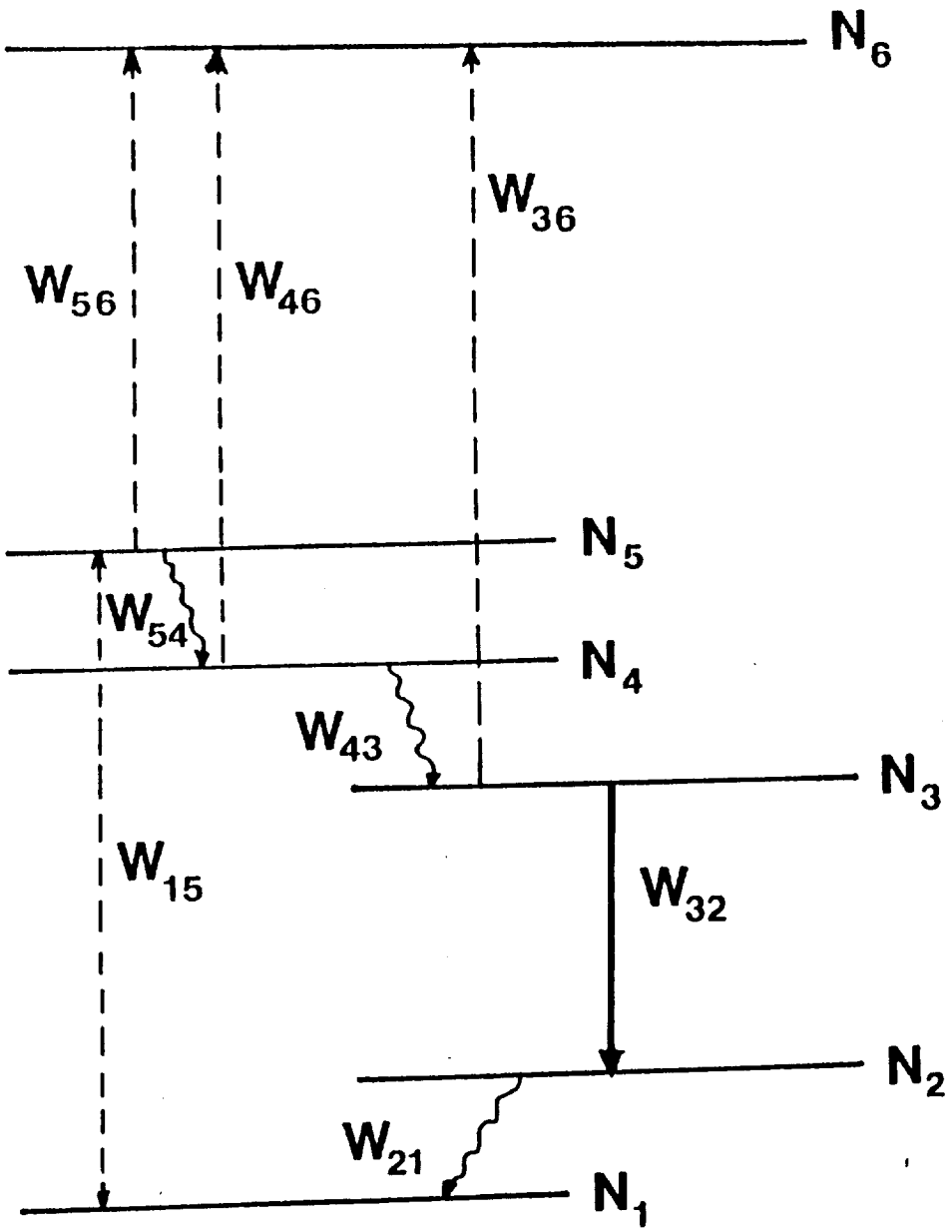

FIG. 2. Schematic used for Rate Equation Model.

a schematic representation of the levels and the transitions considered. The alexandrite laser pumps ions from the ground state (N_1) to the N_5 manifold. Depletion of this level occurs due to relaxation to the metastable N_3 level. Spontaneous and stimulated emission populate the N_2 manifold which then undergoes fast relaxation to the ground state. When there is an energy match between the pump photon and the difference in energy between N_5 and N_6 levels, excited state absorption of the pump photons populates N_6. There is also the situation of pumping into N_5, relaxation into N_4 where ESA of the pump photons occurs, and then further relaxation from N_4 into the metastable state N_3. For non-resonant processes, ESA of the pump photons will occur from the metastable state when there is an energy match between the pump photon and the difference in energy between the metastable state N_3 and an upper excited state N_6.

The rate equations describing the model are

$$\frac{dN_1}{dt} = -W_{15}N_1 + W_{61}N_6 + W_{21}N_2 + W_{51}N_5 \tag{1}$$

$$\frac{dN_2}{dt} = W_{32}N_3 - W_{21}N_2 \tag{2}$$

$$\frac{dN_3}{dt} = W_{43}N_4 - W_{36}N_3 - W_{32}N_3 \tag{3}$$

$$\frac{dN_4}{dt} = W_{54}N_5 - W_{46}N_4 - W_{43}N_4 \tag{4}$$

$$\frac{dN_5}{dt} = W_{15}N_1 - W_{54}N_5 - W_{56}N_5 - W_{51}N_5 \tag{5}$$

$$\frac{dN_6}{dt} = W_{56}N_5 + W_{46}N_4 + W_{36}N_3 - W_{61}N_6 \tag{6}$$

where W_{ij} is the rate of the transition from the i^{th} to the j^{th} level. For fluorescence transitions, W_{ij} is equal to the spontaneous emission rate β_{ij}, and for upward transitions, W_{ij} is equal to $I\sigma_{ij}$ where σ_{ij} is the absorption cross section and I is the peak intensity incident upon the lasing medium.

These equations can be solved for the concentration of ions in the various levels. The pump pulse duration was 60 μs and the nonradiative relaxation to the metastable state was on the order of 1 μs, so steady state conditions were reached in the system in less than 2 % of the pulse duration allowing steady state conditions to be imposed.

The slope efficiency is described by the expression[3]

$$\eta_s = \frac{\lambda_p}{\lambda_o} \cdot (1 - \frac{\sigma_{esa}}{\sigma_e}) \cdot \frac{C_o}{C + L} \cdot \eta_p, \tag{7}$$

where λ_p and λ_o are the pump and output wavelengths, C_o is the output coupler transmission, L is the loss per pass, C is the total transmission of the cavity mirrors, σ_e is the stimulated emission cross section, and σ_{esa} is

the excited state absorption due to lasing photons. The pump efficiency is defined as the fraction of total photons absorbed by the ground state that are converted into excited ions in the metastable state (N_3) and contribute to the laser emission. The pumping efficiency is then written as

$$\eta_p = \eta_p^o \cdot (1 - \frac{d\sigma_{36}N_3 + d\sigma_{46}N_4 + d\sigma_{56}N_5}{d\sigma_{15}N_1}), \tag{8}$$

where d is the diameter of the cavity mode. η_p^o is defined as the pumping efficiency of the material without ESA of pump photons occurring and is usually taken to be unity under the assumption that one absorbed photon creates one excited state.

By applying steady state conditions to Eqs. (3), (4), and (5), the ratios $\frac{N_3}{N_1}$, $\frac{N_4}{N_1}$, and $\frac{N_5}{N_1}$ can be written as

$$\frac{N_3}{N_1} = \frac{\beta_{54}\beta_{43}}{(\beta_{32} + I\sigma_{36})(\beta_{43} + I\sigma_{46})} \cdot \frac{\beta_{15}}{(\beta_{15} + \beta_{54} + I\sigma_{56})}, \tag{9}$$

$$\frac{N_4}{N_1} = \frac{\beta_{54}}{(\beta_{43} + I\sigma_{46})} \cdot \frac{\beta_{15}}{(\beta_{15} + \beta_{54} + I\sigma_{56})}, \tag{10}$$

$$\frac{N_5}{N_1} = \frac{\beta_{15}}{(\beta_{15} + \beta_{54} + I\sigma_{56})}. \tag{11}$$

β_{32} can be written to incorporate both spontaneous and stimulated emission as [4]

$$\beta_{32} = \frac{I_L\sigma_e}{1 + \tau_f\sigma_e I_L}, \tag{12}$$

where τ_f is the fluorescent lifetime of the metastable state and I_L is the intensity of the lasing emission within the cavity. At threshold, $\tau_f \sigma_e I_L \ll 1$, so $\beta_{32} = I_L \sigma_e$, and well above threshold, $\tau_f \sigma_e I_L \gg 1$, so $\beta_{32} = 1/\tau_f$. Since we were considering the case of pumping above threshold, Eq. (12) was estimated with the radiative rate from the metastable level.

The slope efficiency can be rewritten by substituting Eqs. (8), (9), (10), and (11) into Eq. (7) as

$$\eta_s = \eta_s^o \cdot (1 - \frac{A}{I^2\sigma_{15}(\frac{\sigma_{36}}{\beta_{32}})(\frac{\sigma_{46}}{\beta_{43}}) + \sigma_{15} + I\sigma_{15}(\frac{\sigma_{46}}{\beta_{43}}) + I\sigma_{15}(\frac{\sigma_{36}}{\beta_{32}}) + \frac{\beta_{51}}{I} + A}) \quad (13)$$

where

$$A = I^2\sigma_{56}(\frac{\sigma_{36}}{\beta_{32}})(\frac{\sigma_{46}}{\beta_{43}}) + I\sigma_{56}(\frac{\sigma_{36}}{\beta_{32}}) + I\beta_{54}(\frac{\sigma_{36}}{\beta_{32}})(\frac{\sigma_{46}}{\beta_{43}}) + \beta_{54}(\frac{\sigma_{36}}{\beta_{32}}) + I\sigma_{56}(\frac{\sigma_{46}}{\beta_{43}}) + \beta_{54}(\frac{\sigma_{46}}{\beta_{43}}) + \sigma_{56}, \quad (14)$$

and

$$\eta_s^o = \frac{\lambda_p}{\lambda_o} \cdot (1 - \frac{\sigma_{esa}}{\sigma_e}) \cdot \frac{C_o}{C + L} \cdot \eta_p^o. \quad (15)$$

η_s^o and η_p^o were assumed to have a constant value for the different pump wavelengths. All of the values in Eq. (13) are pump wavelength independent except for λ_p but the change in the ratio $\frac{\lambda_p}{\lambda_o}$ is not significant when considering the range of 754 to 791 nm.

There are five simplifications of Eq. (13) to be considered.

Case (1) : If there is no ESA of pump photons, $\sigma_{36} = \sigma_{46} = \sigma_{56} = 0$,

$$\eta_s = \eta_s^o. \tag{16}$$

Case (2) : For the situation where $\sigma_{36} = \sigma_{46} = 0$ and $\sigma_{56} \neq 0$,

$$\eta_s = \eta_s^o \cdot (1 - \frac{1}{1 + \frac{\beta_{54}}{I\sigma_{56}} + \frac{\sigma_{15}}{\sigma_{56}}}). \tag{17}$$

Case (3) : For the situation where $\sigma_{36} = \sigma_{56} = 0$ and $\sigma_{46} \neq 0$,

$$\eta_s = \eta_s^o \cdot (1 - \frac{1}{1 + \frac{\beta_{43}}{I\sigma_{46}} + \frac{I\sigma_{15}}{\beta_{54}} + (\frac{\beta_{43}}{\beta_{54}})(\frac{\sigma_{15}}{\sigma_{46}})}). \tag{18}$$

Case (4) : For the situation where $\sigma_{46} = \sigma_{56} = 0$ and $\sigma_{36} \neq 0$,

$$\eta_s = \eta_s^o \cdot (1 - \frac{1}{1 + \frac{\beta_{32}}{I\sigma_{36}} + \frac{I\sigma_{15}}{\beta_{54}} + (\frac{\beta_{32}}{\beta_{54}})(\frac{\sigma_{15}}{\sigma_{36}})}). \tag{19}$$

Case (5) : For the situation where $\sigma_{36} = 0$ and $\sigma_{46} \neq \sigma_{56} \neq 0$,

$$\eta_s = \eta_s^o \cdot (1 - \frac{1 + (\frac{I\sigma_{56}}{\beta_{54}}) + (\frac{\beta_{43}}{\beta_{54}})(\frac{\sigma_{56}}{\sigma_{46}})}{(\frac{\beta_{43}}{\beta_{54}})(\frac{\sigma_{15}}{\sigma_{46}}) + (\frac{I\sigma_{15}}{\beta_{54}}) + (\frac{\beta_{43}}{I\sigma_{46}}) + 1 + (\frac{\beta_{43}}{\beta_{54}})(\frac{\sigma_{56}}{\sigma_{46}}) + (\frac{I\sigma_{56}}{\beta_{54}})}). \tag{20}$$

Equation (19) reduces to Eq. (17) if $\beta_{43} \gg \beta_{54}$ and $\sigma_{56} \approx \sigma_{46}$. β_{43} and β_{54} are non-radiative rates and were determined from the energy gap law [1,5] and σ_{15} was determined from the absorption spectra and the values for these parameters are given in Table 1.

N (cm^{-3})	1.0×10^{20}	
σ_{32} (cm^2)	7.8×10^{-19}	
λ_o (nm)	1064	
β_{54} (sec^{-1})	2×10^7	
β_{43} (sec^{-1})	7×10^6	
n	1.5	
η_s^o	53 %	
	λ_p=754 nm	
σ_{15} (cm^2)		1.2×10^{-20}
σ_{56} (cm^2)		$3 \pm 1 \times 10^{-18}$
η_s		28 %
	λ_p=791 nm	
σ_{15} (cm^2)		4.4×10^{-21}
σ_{36} (cm^2)		$8 \pm 3 \times 10^{-22}$
η_s		35 %

Table 1: Sample Parameters of Nd-YAG

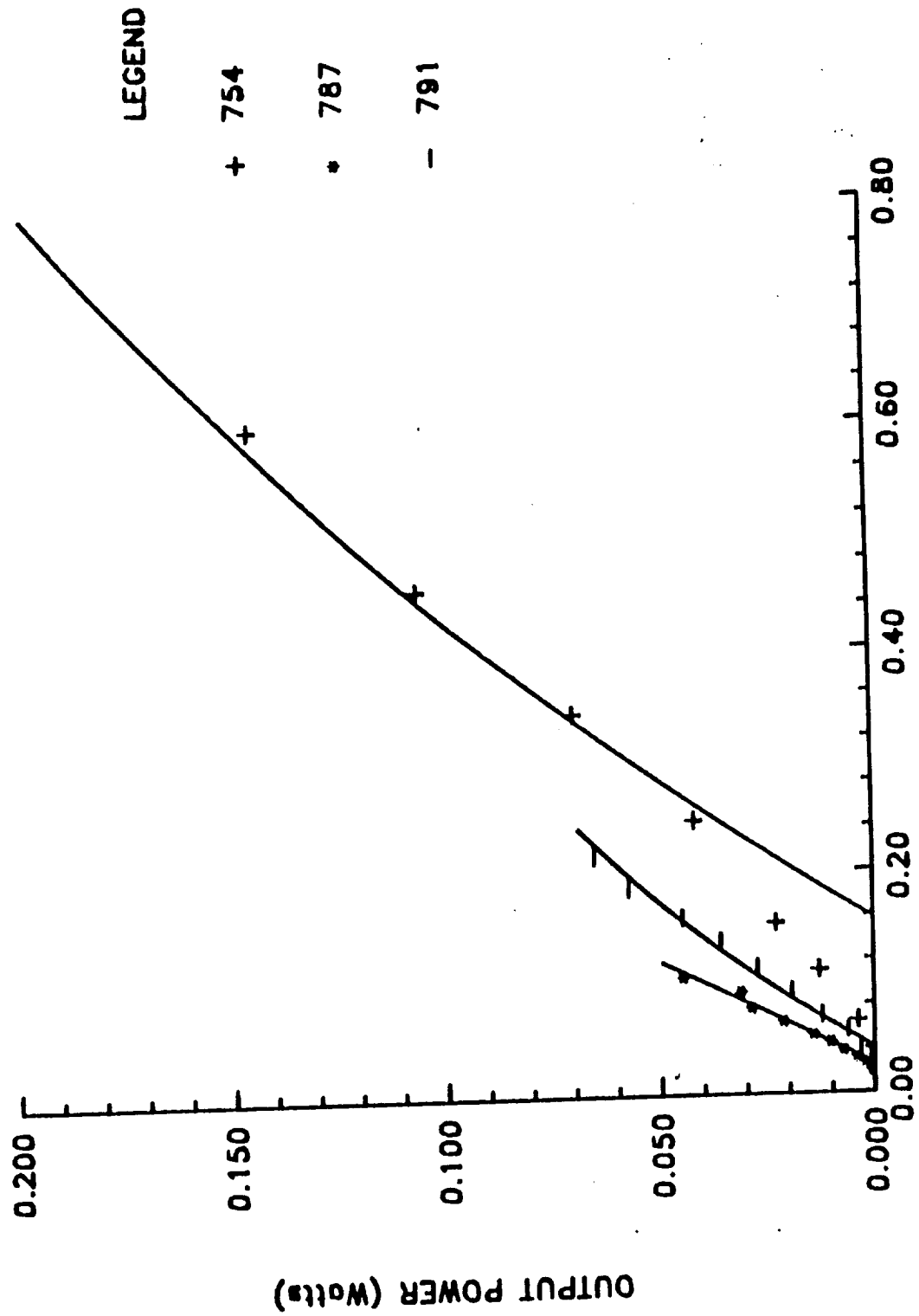

FIG. 3. Power threshold and slope efficiency for Nd-YAG pumped by an alexandrite laser. The solid line is the fit to the slope efficiency curve for 754 and 791 nm pumping.

F.G. 2

The lasing characteristics were measured for three alexandrite pump wavelengths and the slope efficiencies determined. The experimental points are displayed in Fig. 3. The pump wavelengths chosen were characteristic of cases (1), (2), and (4) described previously.

The highest slope efficiency measured was 53 % at a pump wavelength of 787 nm and we assume this corresponds to case (1) of no ESA of pump photons. The energy level diagram (Fig. 1) reveals this wavelength falls outside the overlap region where ESA of pump photons can occur. The box with forward slashes in Fig. 1 is at energies where ESA of pump photons processes can occur and the box with back slashes is at energies where ESA of lasing photon processes can occur. For 754 nm excitation there was a decrease in the slope efficiency and from the energy level diagram it was determined that the resonant ESA process was the dominant process taking place at this pump wavelength. Equation (18) was applied for ESA resonant from a level above the metastable state and an excited state absorption cross section was determined by fitting Eq. (18) to the slope efficiency curve shown in Fig. 3. For 791 nm excitation it was determined that vibronic ESA of the pump photon was the dominant process and an excited state absorption

cross section was determined by fitting Eq. (19) to the slope efficiency curve shown in Fig. 3. The ESA cross sections obtained from the fitting procedure and the values for the parameters used in the calculations are given in Table 1. As expected the excited state absorption cross section for the vibronic process is smaller than that due to the resonant process.

The pumping efficiency discussed in the preceeding section is not the same as the conversion efficiency. The pumping efficiency is defined as the ratio of power out to power absorbed by the ground state of the lasing medium and the conversion efficiency is defined as the ratio of power out to the total power absorbed by the medium. In slope efficiency plots, the power output from the lasing medium is plotted versus the power absorbed by the crystal. When there is no ESA of pump photons the power absorbed by the lasing medium is equal to the power absorbed by the ground state and the pumping efficiency is equal to the conversion efficiency. When ESA of pump photons is present the power absorbed by the medium is greater than the power absorbed by the ground state and this absorbed power cannot be determined from the absorption coefficient of the medium at the specific pump wavelength. It is possible however to find a relationship between the pumping efficiency η_p and

the conversion efficiency η_c. By considering a simple system, one can write the total number of ions that contribute to the laser emission as

$$N_L = N_g - N_{ESA}, \tag{21}$$

where N_g is the number of ions in the ground state that absorb a photon and move to an excited state and N_{ESA} are the number of ions in the excited state that are lost to ESA of pump photon processes. Assuming that one photon absorbed will create one excited state, the pumping efficiency can be written as

$$\eta_p = \frac{N_L}{N_g} = 1 - \frac{N_{ESA}}{N_g}, \tag{22}$$

and this equation is in agreement with Eq. (8) used earlier. The total number of photons absorbed by the material is

$$N_{tot} = N_g + N_{ESA}. \tag{23}$$

Combining Eqs. (21) and (23) the conversion efficiency can be written as

$$\eta_c = \frac{N_L}{N_{tot}} = 1 - \frac{2N_{ESA}}{N_{tot}}. \tag{24}$$

The equation relating the two efficiencies is

$$\eta_c = \frac{\eta_p}{2 - \eta_p}. \tag{25}$$

The conversion efficiency is never greater than the pumping efficiency and the conversion efficiency is useful when determining the wallplug efficiency of the laser.

Discussion and Conclusions

The results discussed above show that alexandrite laser pumped Nd-YAG lasers can have a pump wavelength dependent loss mechanism associated with the excited state absorption of pump photons. This loss mechanism occurs with flashlamp pumping but its consequences are magnified when pumping laser materials with monochromatic light. ESA of pump photons will occur for transitions resonant from upper levels and vibronic transitions from the metastable state. It will limit the slope efficiencies obtainable by as much as 50 % in rare earth doped laser materials and complete characterization of the pumping dynamics must be determined in order to limit this loss mechanism. It is also possible to obtain an estimate for the excited state absorption cross section from the rate equation model.

Different processes which effect the slope efficiency such as thermal lensing and ground state saturation were not accounted for in this rate equation

model. ESA of the pump photons will cause the crystal to store heat and this may be one reason for the large heat load reported when flashlamp pumping Nd-YAG. Heat storage in the laser material will also cause a greater amount of thermal lensing in some materials and the thermal lensing will decrease the value of the slope efficiency further. The resulting excited state absorption cross section determined from the above method must be considered as a upper limit since it is assumed that only ESA of pump photons is causing the change and it might be a combination of ESA of pump photons and other processes.

An approximation that is made in this method is the calculation of the nonradiative relaxation rate from the Energy Gap law. The Energy Gap law fails as small energy gaps are approached because the approximation that the nonradiative relaxation rate follows an exponential is no longer a valid assumption. The calculation of the excited state absorption cross section is very dependent upon the nonrelaxation rate and any inaccuracies are carried through to the value of σ_{ESA}. It is difficult to use this technique to determine the excited state absorption cross section in disordered materials or in materials where the nonradiative relaxation rate is not known.

Figure 4 shows the energy levels of Nd^{3+} in various hosts. The resonances needed for ESA of pump photons to occur is very host dependent because of the shifts in energy levels and strengths of the transitions to the $^2D_{1/2}$, $^2P_{3/2}$, and $^2P_{1/2}$ levels. Thus by carefully choosing the host material, ESA of the pump photons can be maximized or minimized. If ESA of pump photons is maximized in solid state laser materials it might be possible to lase the transition from the highest excited state to the ground state thus producing a green or possibly a blue solid state laser using this type of pumping scheme. For example, the disordered hosts such as BMAG appear to have strong ESA of pump photons due to their broadened energy levels resulting in a greater probability of energy match with pump photons.[6] On the other hand, crystals such as Nd:YVO_4 appear to have a weak transition probibility to the level needed for ESA of pump photons to occur when pumping into the $^4F_{7/2} + ^4S_{3/2}$ and $^2H_{9/2} + ^4F_{5/2}$ manifolds.[7]

This theory for ESA of pump photons presented is not limited to Nd^{3+}. Fluorescence observed in Er^{3+} and Ho^{3+} -doped laser materials when pumping with the emission of an alexandrite laser can be explained with this mechanism. The strength of this process will be determined by the resonance of

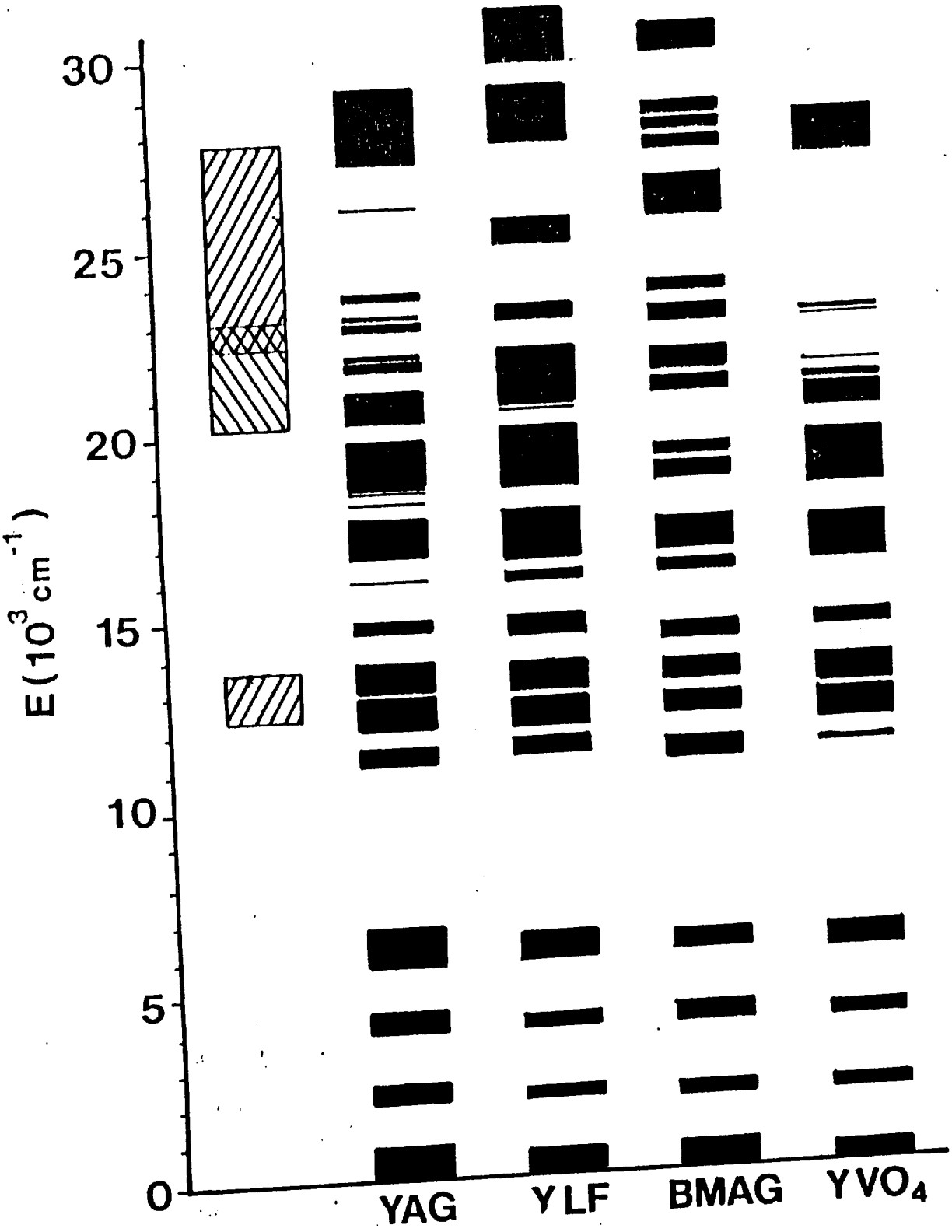

FIG. 4. Energy levels of Nd^{3+} in $Y_3Al_5O_{12}$ (YAG), $LiYF_4$ (YLF), $Ba_2MgGe_2O_7$ (BMAG), and YVO_4.

the energy of the pump photons wwith the energy difference of energy levels of the impurity ion.

References

[1]M.L.Kliewer and R.C.Powell, *IEEE J.Quant.Electron.*, **QE-24**, 5016 (1989).

[2]A.E.Seigman, *Lasers*, University Science, Palo Alto, 1986.

[3]J.A.Caird, S.A.Payne, P.R.Staver, A.J. Ramponi, L.L.Chase, and W.F.Krupke, *IEEE J.Quant.Electron.*, **QE-24**, 1099 (1988).

[4]W.Koechner,*Solid-State Laser Engineering*, Springer-Verlag, New York, 1976.

[5]L.A.Riseberg and M.J.Weber, *Progress in Optics*, **14**, pp. 89-159, (1977).

[6]M.J.Ferry, R.J.Reeves, M.L.Kliewer, T.Allick, and R.C.Powell, to be published.

[7]M.L.Kliewer, L.G.Deshazer, and R.C. Powell, to be published.

III. CRYSTAL GROWTH

A. INTRODUCTION

The scheelite structure compound $LiYF_4$, known by the acronym YLF, is an excellent host for trivalent rare earths. Single crystal can be grown by the Bridgman[1] method and by pulling from the melt[2,3]. Both techniques are made somewhat more difficult because YLF melts incongruently; at 819°C it transforms first to YF3 and liquid. Consequently, crystals are grown from melts containing a few percent excess LiF. The pulling of YLF crystals from the melt should be considered as "top-seeded solution growth" rather than the Czochralski method. We are using both the Bridgman method and the pulling method to grow doped YLF crystals.

We have found that HF treated starting materials must be used for both crystal growth methods. The materials are prepared from a mixture consisting of 52% chunks of single crystal LiF and the remaining 48% consists of YF_3 plus the appropriate amount of ErF_3 or other rare earth dopant. The mixture is then heated to about 900°C in a flowing Ar/HF atmosphere. The HF treatment cleans up the oxides, carbonates, and hydroxides remaining in the material. This treatment produces a fine grain polycrystalline mixture that is then used for the actual crystal growth run.

The major implication of the incongruently melting nature of YLF for pulling crystals from the melt is that all changes must be made slowly so that the melt can "adjust" to the new conditions. We have modified our pulling system so that the temperature is computer controlled with the ability to make steps as small as 0.2°C. The computer system significantly

reduces the amount of operator intervention needed to pull crystals. In the next section, we will describe our current approach to pulling crystals. We are also preparing YLF double doped with mixtures of Er and Pr, and Er and Dy. The intent of the second dopant is to provide a more efficient laser diode pumping scheme.

B. RESULTS AND DISCUSSION

Figure 1 shows the computer controlled temperature versus time profile for YLF:Er run number 062689. The temperatures given in Fig. 1 are the control temperature of the tungsten mesh heater used in our crystal puller and not the actual temperature of the melt. At time zero in Fig. 1 (late in the afternoon) the seed was dipped into the melt at the starting control temperature of 864^{o}C. Shortly after the dipping the seed, the pulling rate of 0.75 mm/hr was established and the furnace temperature was starting down at a rate of 1^{o}C/hr (0.2^{o} steps). Three hours later (around 8 pm) the cooling rate was changed to 0.5^{o}C/hr for the unattended overnight portion of the run. During this time the crystal came out to its final diameter of about 0.7 cm. At 14 hours into the run (the next morning) the temperature was held constant and the lift rate increased to 1 mm/hr. The crystal diameter then held steady for the remaining 6 hours of the run. The crystal was "traced" onto the upper portion of Fig. 1. Since the melt level goes down as the crystal is pulled the actual growth rate is larger than the lift rate. With this control system we believe that we can reliably grow doped YLF holding a reasonably constant diameter up to diameters of 1.2 to 1.5 cm. In our system, larger diameters become unstable and the addition

of some type of direct diameter control is necessary.

We occasionally see a few grain boundaries in crystals such as the one described above. Recently, we have found that it is advantageous to start the growth run near 870°C and "neck" the seed in before growing out to the desired diameter. We are in the process of refining the control scheme for this process.

C. REFERENCES

1. W. A. Shand, J. Crystal Growth, 5, 143 (1969).

2. B. Cockyane, J. G. Plant, and R. A. Clay, J. Crystal Growth, 54, 407 (1981).

3. R. Uhrin, R. F. Belt, and V. Rosati, J. Crystal Growth, 38, 38 (1977).

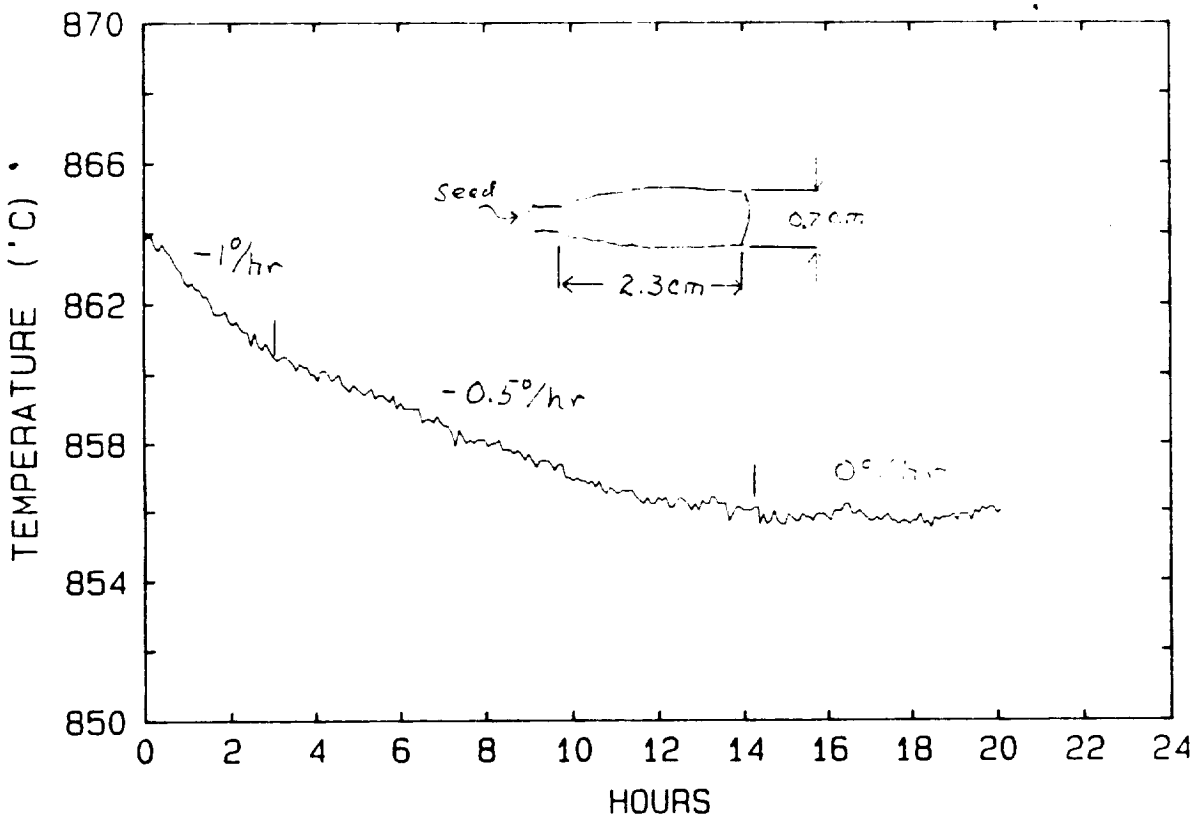

Figure 1. The control temperature versus time profile used during YLF:Er growth run 062689 is shown. The inset is a "tracing" of the resulting crystal.

IV. RADIATION DAMAGE

A. INTRODUCTION

In laser hosts and other insulating crystals ionizing radiation produces free electrons and holes. While these free carriers have only a very short lifetime they can interact with the intrinsic ions and with the dopants to produce a variety of defects. Some of these radiation-induced defects may degrade the performance of the laser. In fluorides (and alkali halides) a free hole combines with a pair of adjacent fluorines to form an excited F_2^- molecule. This excited center is often referred to as a V_K center. These excited molecules are only stable at low temperatures; at room temperature they quickly decay. The decay products usually take the form of a fluorine vacancy containing a trapped electron and fluorine interstitial clusters. The fluorine vacancy with a trapped electron is the traditional F-center of color center physics and usually has an absorption band in the near-uv region. F-centers are are relatively mobile and depending upon the crystal structure, temperature, and their exposure to to light they often combine to form F-aggregate centers. The F_2-center (not to be confused with the F_2^- molecule or V_K center) which is also known as the M-center consists of of a pair of nearest-neighbor F-centers. The F_3 center or R-center consists of three neighboring F-centers. In fluorides, these aggregate centers usually have absorption bands in the blue to near-uv regions. Very little work has been done on radiation effects in $LiYF_4$ (YLF). Renfro,*et al.*[1] reported that several different color centers were produced in both undoped and erbium doped YLF by irradiation at low temperatures. Their study

concentrated on the characterization of the paramagnetic $\dot{V}_K$ center which is the precursor of the F-centers. The V_K centers were produced by bleaching a previously low temperature irradiated sample with uv light. The V_K center has an absorption band at 338 nm which is strongly polarized parallel to the c-axis. The center annealed out when the sample was warmed above 120 K. They also suggested that a partially polarized band at 335 nm was the conventional F-center. We report here some new results of our investigation of radiation effects in both undoped and doped YLF.

B. RESULTS AND DISCUSSION

Samples for the radiation studies were 1.5 mm to 2 mm thick slices taken from both undoped and Er doped Bridgman grown crystals. The samples were oriented with the c-axis in the plane of the slice. The irradiations were carried out using either a 1.75 MeV electron Van de Graaff source or a 18 krad/hr ^{60}Co gamma source. Optical absorption measurements were made as a function of irradiation time using a Perkin-Elmer Model 330 spectrophotometer. The color center bands were slightly narrower when measured at 80 K and all of the reported spectra were taken at this low temperature.

As shown by the middle curve in Figure 1 a 120 sec electron irradiation of an undoped YLF crystal produced color center bands at 1.95 eV, 2.28 eV, 2.9 eV, 3.7 eV, and a broad band above 4 eV. The 3.7 eV band was previously assigned to the F-center[1]. The high energy band probably consists of overlapping bands; one at 4.5 eV and the other at 4.85 eV. When the irradiation was continued to a total time of 900 sec all of the bands grew as

shown by the upper curve in Fig. 1. At 900 seconds the total radiation dose is estimated to be around 80 Mrad. The assignment of the other radiation-induced absorption bands to has not yet been made. The fluorine ion occupies several different sites in YLF, and there should be more than one type of F-center. Some of the bands should also be due to F-aggregate centers.

Figures 2 and 3 show the growth of these bands with radiation time. The production curves show a rapid early stage coloration followed by a much slower growth at larger doses. The general shape of the production curves is consistent with earlier results for other fluoride crystals. F-aggregate centers are expected to grow in at rates different than that of the F-center. For example, the M center should grow in proportional to the square of the F-center concentration^2. No large production differences were observed between the different bands. Consequently, at this stage of the investigation assignments of the various bands remain uncertain.

The color centers produced by irradiation at room temperature start to anneal immediately. The dashed curve in Fig. 4 shows the absorption spectrum taken on the undoped YLF sample immediately after the 900 second irradiation. The solid curve which was measured 36 hours later shows that the 1.95 eV band has grown, the 2.28 eV band has completely disappeared, and that the higher energy bands show a small decrease. This sample was subsequently used for an isochronal anneal study. The sample was heated to a given temperature, held there for 5 minutes, cooled quickly back to room temperature and remeasured. Figure 5 shows the resulting anneal curves. The 1.95 eV band grew

slightly for temperatures up to 150°C and then quickly decayed. The 2.8 eV, 3.7 eV F-center, and 4.5 eV bands all decayed smoothly over the 30° to 250°C range shown in Fig. 5. The 4.85 eV band tracked with the 4.5 eV band and was omitted from Fig. 5 for purposes of clarity. In $RbMgF_3$, the F-center does not start to anneal until about 230°C and its anneal is matched by the growth of the R-center which peaks at 370°C and then goes out[3]. Low temperature thermal conductivity results for irradiated $RbMgF_3$ suggest that the radiation-induced fluorine interstitials form large clusters (approximately 2000 atoms). These large clusters may cause the F-centers to remain stable to higher temperatures. If this speculation holds then we might expect the interstitial clusters in YLF to be much smaller.

Figure 6 compares the as-received spectrum of a YLF sample doped with 2% erbium with the spectrum observed after it was gamma irradiated to a dose of 3.6 Mrad. The color center bands that we see in the irradiated undoped crystal are superimposed upon the erbium spectrum. No color center absorption bands were observed at lower energies. The 1.95 eV band does not seem to be present in this gamma irradiated sample (perhaps it is masked by the erbium band).

C. REFERENCES.

1. G. M Renfro, L. E. Halliburton, W. A. Sibley, and R. F. Belt, J. Phys. C: Solid St. Phys., 13, 1941 (1980).
2. C. R. Riley and W. A. Sibley, Phys. Rev. B., 1, 2789 (1970).
3. N. Koumvakalis and W. A. Sibley, Phys. Rev. B., 13, 4509 (1976).
4. J. B. Hartmann and J. J. Martin, Phys. Stat. Sol. (b), 84, 721 (1977).

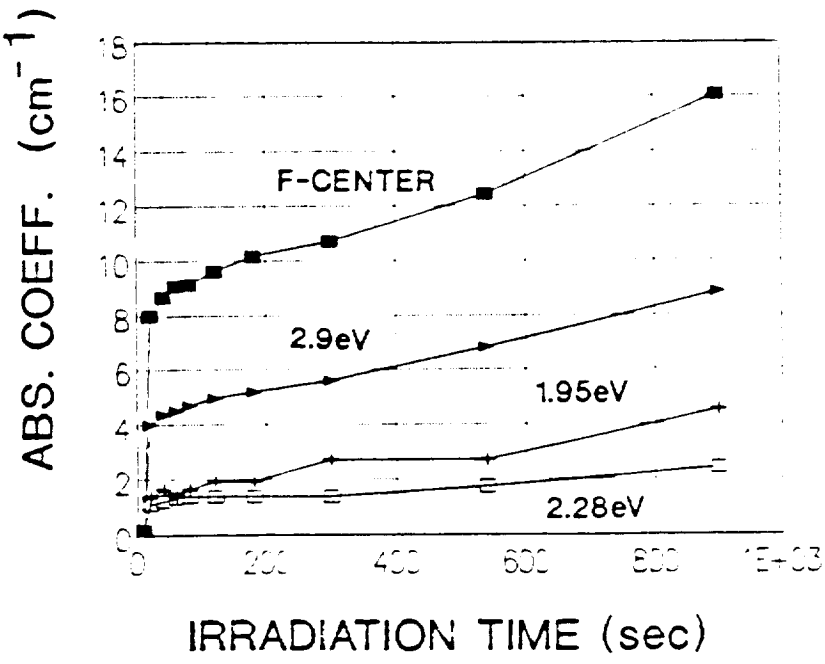

Figure 2. The production curves for the lower energy color center bands are shown.

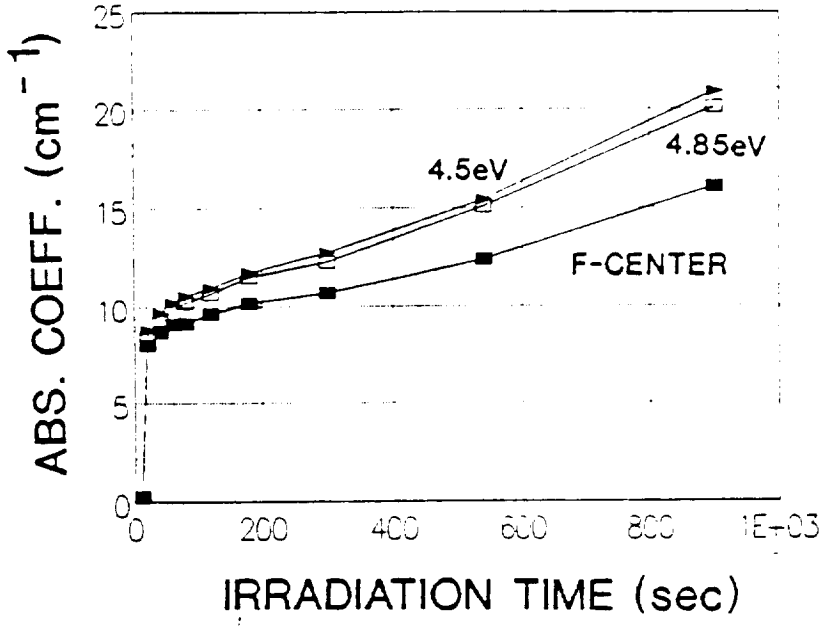

Figure 3. The production curves for the 4.5 and 4.85 eV bands and the 3.7 eV F-center band are shown.

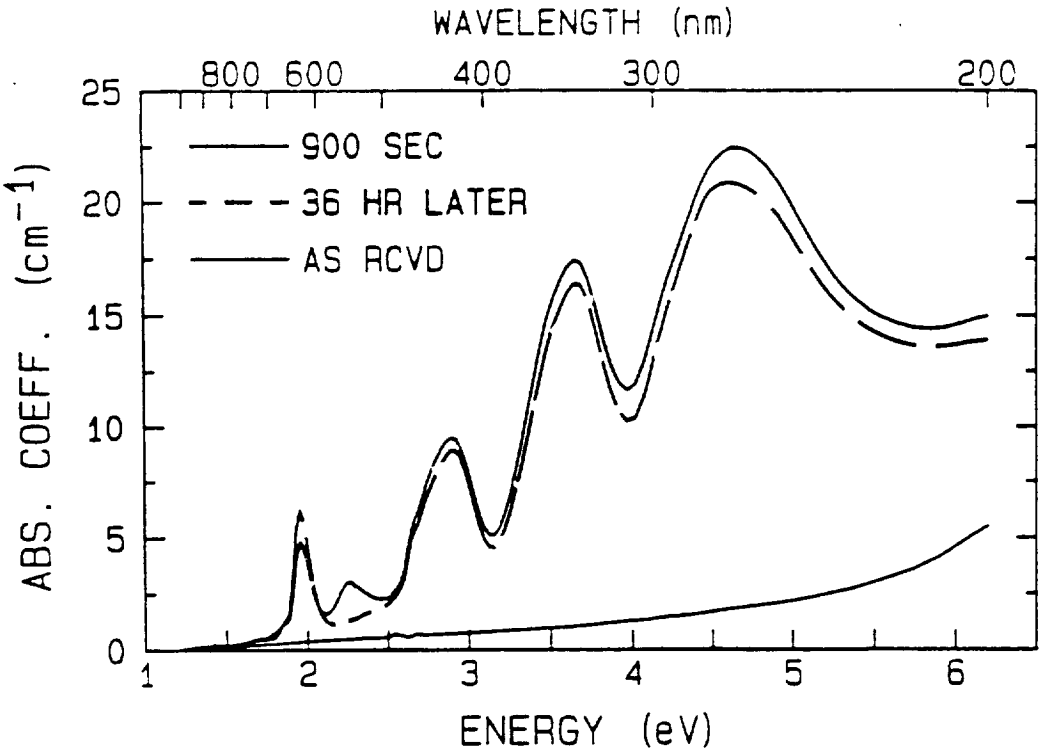

Fig. 4. After 36 hours at room temperature the 2.28 eV band disappears and the 1.95 eV band grows. The other bands decay slightly.

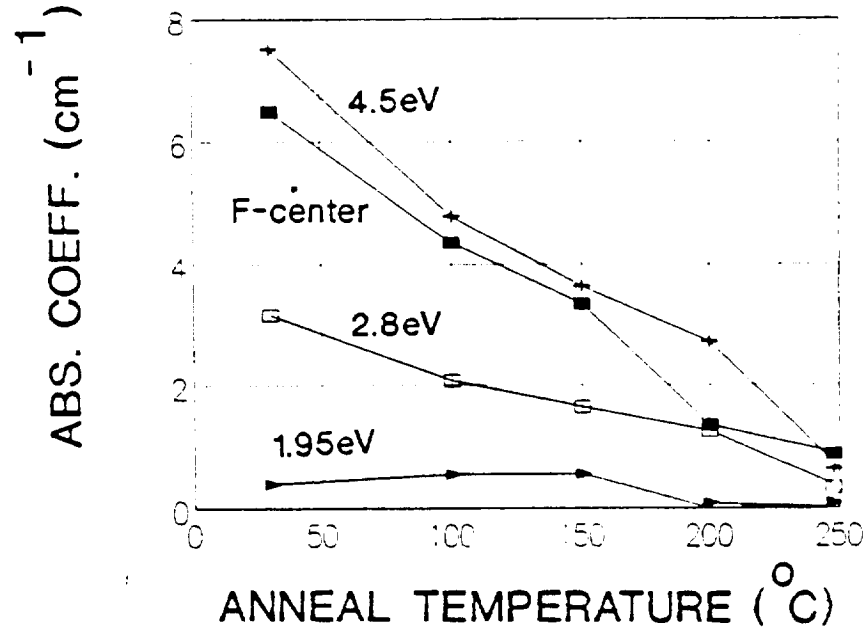

Figure 5. The isochronal anneal curves for the color center bands are shown.

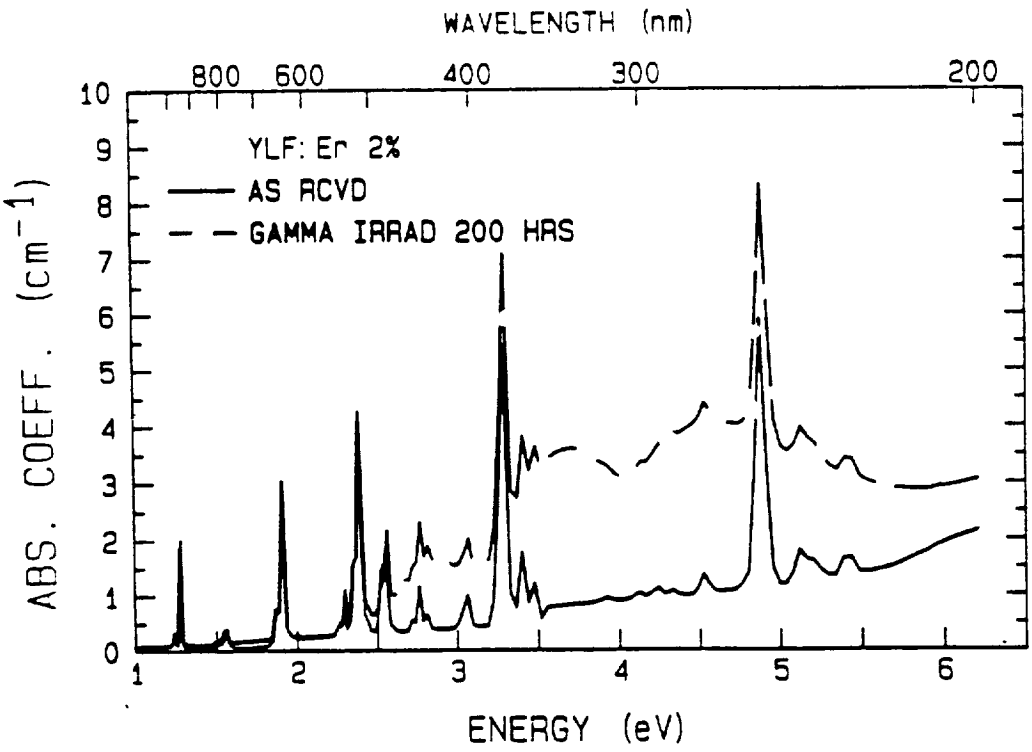

Figure 6. The color center bands are superimposed upon the erbium spectrum by irradiation.

NASA
FORMAL
REPORT

FFNo 665 Aug 65